Binding Angle Robustness of Plasmonic Nanorod Dimer Resonances

Andreas Hohenau, Matthieu Bugnet, Viktor Kapetanovic, Guillaume Radtke, Gianluigi A. Botton, Nikita Reichelt, Ulrich Hohenester, Joachim R. Krenn, Leïla Boubekeur-Lecaque, Nordin Felidj

RESEARCH ARTICLE

ADVANCED OPTICAL MATERIALS
www.advopticalmat.de

Binding Angle Robustness of Plasmonic Nanorod Dimer Resonances

*Andreas Hohenau, Matthieu Bugnet, Viktor Kapetanovic, Guillaume Radtke, Gianluigi A. Botton, Nikita Reichelt, Ulrich Hohenester, Joachim R. Krenn, Leïla Boubekeur-Lecaque, and Nordin Félidj**

Narrow gaps between coupled plasmonic nano-particles show strong optical field enhancements and spectrally adjustable resonance positions, making them attractive for surface enhanced spectroscopies. Gold nanorod dimers formed from nanorod solutions with narrow size distributions are intensely investigated in this context. However, the binding angle of rods coupled at their end faces is usually not controllable. Surprisingly, it is observed that this has only little effect on field enhancement and resonance energies. In this work, gold nanorod dimers are investigated by mapping their plasmon resonances using electron energy-loss spectroscopy in a scanning transmission electron microscope. For a wide range of dimer orientations, a negligible influence of the angle between the two rods on the bonding and antibonding longitudinal dipole resonances is confirmed, in good agreement with numerical simulations. The results are interpreted via the predominant end-coupling of the individual nanorod's plasmonic modes, as illustrated by an analytical charge coupling model. In addition, the simulations emphasize that conclusions from experimental data on the gap morphology on the size range of one nanometer can be ambiguous. In any case, the full understanding of the angle-invariant resonances of nano-rod dimers can further promote their controlled application in surface enhanced spectroscopy or -sensing.

1. Introduction

Nano-scale gaps formed by plasmonic nano-particles can generate strong local electromagnetic fields if excited with light matching the frequency of the localized surface plasmon resonance (LSPR). These fields are spectrally tunable via the used metal, the geometry parameters of the particles and the dimensions of the gap.[1] Due to the resonant character of the plasmon excitation, the gap fields can be strongly enhanced with respect to the exciting light field. Enhanced gap fields are thus of high interest for surface enhanced spectroscopies, sensing, strong light/matter coupling or nonlinear optics.[2] With ultrasensitive sensor applications in mind, two further aspects should be considered. First, it is appealing to have a large number of particles and thus gaps available (or an easily adjustable density thereof), which makes particles in solution preferable to surface-bound structures for many applications. Second, the plasmonic gap mode should be spectrally tunable to an analyte of choice, preferably via the particle geometry so that the gap size can be kept fixed.[3] Prominent and well-investigated particles for gap formation are gold nanorods.[4] The strong curvature at the nanorod ends can be exploited for high-yield end-to-end dimerization of individual rods,[5,6] whereas the resonance position can be tuned by the nanorod length. This comes, however, at a price, as

A. Hohenau, N. Reichelt, U. Hohenester, J. R. Krenn
Institute of Physics
University of Graz
Universitätsplatz 5, Graz 8010, Austria

M. Bugnet
CNRS
INSA Lyon
Université Claude Bernard Lyon 1, MATEIS, UMR 5510, Villeurbanne 69621, France

The ORCID identification number(s) for the author(s) of this article can be found under https://doi.org/10.1002/adom.202400929

DOI: 10.1002/adom.202400929

M. Bugnet, V. Kapetanovic, G. A. Botton
Department of Materials Science and Engineering
McMaster University
1280 Main Street West, Hamilton, Ontario L8S 4L7, Canada

G. Radtke
Sorbonne Université, CNRS UMR 7590, MNHN
Institut de Minéralogie, de Physique des Matériaux et de Cosmochimie (IMPMC)
4 place Jussieu, CEDEX 05, Paris 75252, France

L. Boubekeur-Lecaque, N. Félidj
Université Paris Cité
ITODYS, CNRS, Paris F-75006, France
E-mail: nordin.felidj@univ-paris-diderot.fr

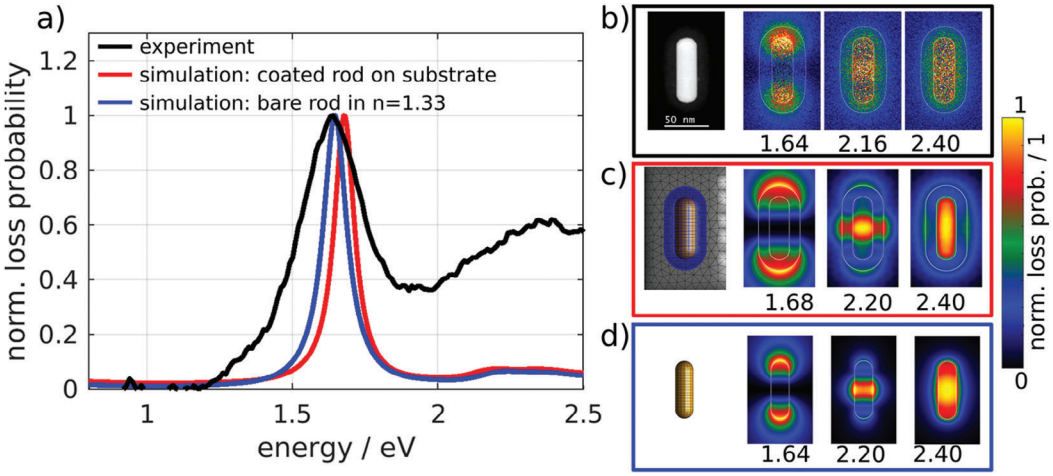

Figure 1. a) Measured (black) and simulated (red: coated, on carbon film; blue: bare, in homogeneous environment with $n = 1.33$) EEL spectra. The experimental spectrum was integrated over the nanorod (for position resolved spectra and effects of contamination see Figure S2, Supporting Information) whereas the simulated spectrum is for an electron beam position 5 nm from the rod end on its axis. b) STEM-ADF image and measured EEL maps at 1.64, 2.16, and 2.4 eV. c) Model and simulated EEL maps of a nanorod with a 14 nm thick silica coating on a 2 nm thick carbon substrate. d) Model and EEL maps of a nanorod in homogeneous environment with $n = 1.33$.

the mutual orientation of both rods that is set upon binding varies statistically. At first view, this can be suspected of giving rise to different spectral signatures due to different gap morphologies.[7] However, with some controversy[8] it was shown, that the resonance energy of the coupled dipolar resonance of metal nanorod dimers is largely independent of the binding angle.[9] Although nominally similarly sized particle pairs with different binding angles were compared, strong scattering in the experimental data due to variations in particle shape and dimer distance led to about 100 nm of uncertainty in resonance wavelength.[9] In particular, variations in the binding distance of randomly arranged dimers pose a major limitation in terms of maintaining a constant resonance position, as there is a roughly exponential relation between spectral resonance shift and particle distance.[10]

To allow for an unambiguous comparison of experiments to simulations and to identify underlying physical principles of the surprising invariance of LSPR against variations in the binding angle, nanorod dimers are needed that have a well-defined constant binding distance but varying binding angles. Moreover, they should be stable enough to allow spectral and spatial mapping of the underlying LSPR modes by electron energy loss spectroscopy (EELS) in scanning transmission electron microscopy (STEM).[11–14] Recently, we developed a strategy to obtain stable gold nanorod dimers in solution,[6] where two nanorods are linked by BPE (1,2-Bis(4-pyridyl)ethylene) that acts as bifunctional linker- and spacer molecule. Subsequent encapsulation in a silica shell produces highly stable dimers with an expected gap width of about 1 nm that can withstand drying after drop-casting onto a surface, making them suitable for investigation by STEM-EELS mapping. Carbon contamination eventually forming during STEM on the surface of plasmonic nanoparticles has non-negligible influence on the plasmonic resonances, however, the silica coating used here also prevents carbon contamination to reach the gold nanorods surfaces, thereby reducing this effect.

In the following, we present EEL spectra and energy-filtered surface plasmon resonance maps of silica-coated gold nanorod dimers on an ultra-thin carbon film. The measured resonance energies of the bonding and antibonding longitudinal dipolar plasmons are virtually independent on the binding angle of the rods. Numerical simulations confirm these observations, but highlight as well that conclusions on the nano-scale gap morphology (open or closed gap, pristine hemispherical end caps or interaction-induced flattening) have to be handled with great care. We complement these results with an analytical model of charge coupling, emphasizing the predominant end-coupling of the individual nanorods.

2. Results and Discussion

2.1. Nanorod Monomer

We start our analysis with a close look on a single gold nanorod with a length of 82 nm, a diameter of 25 nm and a silica layer thickness of 14 nm (see Figure S1, Supporting Information) deposited on a 2 nm thick carbon substrate (STEM annular dark field (ADF) image in **Figure 1b**). In the experimental EEL spectrum (Figure 1a), we observe two resonance peaks at 1.70 and 2.40 eV. The comparison to simulations shows good agreement and allows to attribute the 1.70 eV resonance to a longitudinal dipolar mode (LDM). At 2.20 eV, a quadrupolar resonance is found in the simulations. The corresponding loss probability is less than 10% of the peak at 1.70 eV, however it can be discerned also in the experimental EEL map at 2.16 eV. The weak resonance peak found in the simulations around 2.4 eV (520 nm) is at the onset of the gold d-band absorption and the limiting energy where spectrally overlapping, strongly damped resonances of different higher orders pile up. The experimental and simulated EEL maps (Figure 1b–d) indeed do not show any pronounced pattern around 2.4 eV, but the EEL probability is rather uniform across the particle and quite confined within its borders.

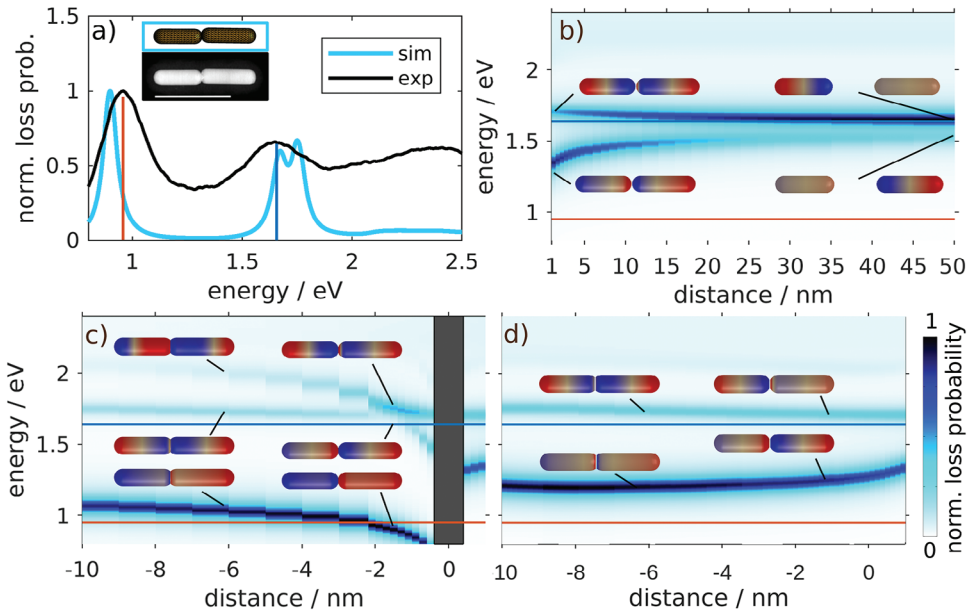

Figure 2. a) Measured and simulated EEL spectra for the near end-to-end configuration. The orange and blue lines mark the experimental peak maxima, corresponding to the horizontal lines in b–d). Inset: STEM-ADF image and model shape. The experimental spectrum was integrated over the dimer whereas the simulated spectrum is an average over three electron beam positions as indicated in Figure S3, Supporting Information. b) Distance dependence of exactly aligned nanorods with dimensions fitting the experimental case in a), distance range 1 to 50 nm. At 50 nm distance the modes are basically uncoupled. The resonance energies correspond to those of the shorter and longer rod, respectively. c) as b), but in the distance range between -10 (fused, conductive contact) and 1 nm. The distance range between -0.4 and 0.4 nm is grayed out, as simulations in this range would only make sense when including tunneling effects. d) as b), but with a constant gap width of 1 nm maintained by flattening the nanorod ends accordingly. Insets: charge distribution of the corresponding quasi-static eigen-modes. The orange and blue lines indicate the experimentally observed resonance positions at 0.95 and 1.64 eV.

For the simulations of the more complex geometries considered later in this work, we try to simplify the system by replacing the coating and substrate by a homogeneous environment of constant refractive index. A value of $n = 1.33$ was found to give good agreement with the experimentally observed resonance energy. In Figure 1b–d the experimentally recorded and simulated EELS maps are compared. Whereas the model with coating somehow reproduces the experimentally observed losses within the shell region (compare Figure 1b,c at 2.40 eV), the high loss probability visible at the outer shell surface at 1.68 eV in Figure1c is not found experimentally. A possible explanation for this might be the approximate modeling of the silica coating by the homogeneous dielectric function of SiO_2.[15] If the shell is replaced by a homogeneous environment (Figure 1d), the region of high loss probability is, in comparison to the experiments, a little too confined to the gold region. Nevertheless, the accordance between simulations and experiment is quite good, and we will use an homogeneous environment with $n = 1.33$ in the following simulations.

2.2. Nanorod Dimers

When combining two nanorods to a nanorod dimer, the plasmonic modes on both rods start to couple via their electromagnetic fields. For simplicity we first consider two rods of identical diameter (21 nm) and co-linear axes (end-to-end configuration) in homogeneous environment ($n = 1.33$), as depicted in the inset **Figure** 2a. Here, the lengths of the two nanorods are 79 and 70 nm, similar to the experimentally investigated dimer No. 1 (Figure S4 and Table S1, Supporting Information). The experimentally recorded EELS spectrum depicted in Figure 2a shows two clearly discernible resonances at 0.95 and 1.64 eV that can be attributed to plasmon excitations. As for the monomer, the additional broad peak at about 2.40 eV coincides with the onset of the gold d-band absorption and the higher order pile-up. The measured energies of the two plasmonic resonances are plotted as the horizontal orange and blue lines in Figure 2b–d.

Corresponding to the experimental case, we use the rod lengths of 79 and 70 nm in the following simulations. The simulated EEL spectrum in Figure 2a is in good agreement with the experiment and shows a double peak at the high energy resonance, which will be addressed below. In Figure 2b we depict how the EEL spectra evolve as a function of end-to-end distance. At a distance of 50 nm, the coupling is relatively weak and the EEL spectrum shows two peaks at 1.52 and 1.65 eV, corresponding to the resonance positions of the shorter and longer rods of the dimer, respectively. The modes are strongly localized on one rod only (insets, Figure 2b, right side). With decreasing end-to-end distance, the coupling becomes more pronounced and the low energy mode shifts to the red, whereas the high energy mode shifts (to a lower extend) to the blue. At a distance of 1 nm, the modes are strongly coupled (hybridized), and are better described as a bonding dipole mode (BDM) and an antibonding dipole mode (ADM, insets, Figure 2b, left side). When the rods are overlapping (negative distances, Figure 2c), i.e., here

their hemispherical caps merge, three prominent modes are observed. Exemplary for $d = -1$ nm, the lowest energy mode at 0.92 eV is the charge transfer mode. This is followed by a mode with a charge distribution similar to the BDM of separated rods (1.66 eV). The mode at 1.75 eV resembles that of the ADM. For a larger overlap of 6 nm, the charge transfer mode is found at 1.04 eV, followed by modes at 1.74 and 2.01 eV. The influence of the constriction where the rods touch becomes less pronounced for increasing overlap and the mode patterns approach those expected for a single long nanorod. Note that we exclude the distance range −0.4 to 0.4 nm where tunneling effects have to be considered.[3]

Interestingly, for the geometries considered so far, the experimental peak energies (orange and blue lines in Figure 2) only fit to the simulated spectra for nanorods in conductive contact in the range around −1.5 nm. If the full experimental situation is simulated, including the presence of the silica shell and the substrate, the fit is even better (Figure S5, Supporting Information). The STEM ADF image of the investigated dimer (inset in Figure 2a) as well shows seemingly overlapping nanorods. However, the dimerization process where the dimers are formed and held together only by the linker molecules, is expected to yield consistent 1 nm wide gaps. Indeed, STEM images of linked dimers without silica coating allow to image this gap.[6] The silica coating is not expected to influence the linker molecules. Surface enhanced Raman spectra of silica coated end-coupled nanorod dimers in solution seem to confirm the presence of the linker molecule after coating and thus also the presence of the gap. As the silica coating stabilizes the binding angles and the gap width, coated dimers (in contrast to the uncoated dimers) are generally not deposited on the substrate in a planar configuration. It could be expected that an (apparent) overlap is due to the projection of a 3D configuration onto a 2D image, with an inclined gap with respect to the electron beam direction. Thus, although the dimer looks like overlapping, the presence of a gap seems likely. Moreover, the actual nanorod end faces are actually not hemispherical but faceted[16] and it is known from other configurations that upon binding the particle ends flatten off,[17] forming an extended flat gap region of constant width.

To clarify this point, we also simulate the distance dependence for flattened rod ends. Distances below 1 nm correspond to geometries similar to the conductively contacting dimers in Figure 2c but with accordingly flattened nanorod end faces to maintain a physical gap widths of 1 nm (Figure 2d). Here, we observe a continuous transition of the resonance energies. The bonding dipole mode first shows a red-shift due to the increased coupling strength to the opposing, flat surfaces of increasing size. Only below about −9 nm this trend is reversed and the blue shift caused by the shortening of the nanorods upon flattening of their ends begins to dominate. The antibonding dipole mode at about 1.70 eV in contrast shows a monotonous, weak blue shift with decreasing distances over the entire range, caused by the enforced coupling and shortening of the rods. Evidently, the resonance energies of rod dimers with 1 nm gap and flattened ends do not fit the experimental observation for any distance. Adjustments in the assumed simulation parameters, such as decreasing the gap width, increasing the refractive index of the assumed dielectric environment and/or considering more elongated nanorods shift the resonance positions closer to the experimental ones (see Figure S6, Supporting Information). EEL-maps at the resonance energies for various gap geometries show no pronounced differences as well (see Figure S7, Supporting Information) and thus robust conclusions regarding the gap morphology at the 1 nm scale cannot be drawn within the scope of this work.

The experimental EEL maps at the observed resonance energies show good agreement with the simulations of connected rod ends (**Figure 3**). We use these maps to clarify the discrepancy between the experimental and simulated data in Figure 2a, where we measured one feature at 1.69 eV, while two resonance peaks at 1.67 and 1.76 eV were identified by the simulation. This observation is most likely due to the limited experimental energy resolution, as well as potential beam-induced changes at the interface between the metal and the shell resulting in the alteration of the local dielectric environment and subsequent shifts of the plasmonic modes[18] (see Figure S8, Supporting Information). Summing-up both simulated EEL maps for the energies of 1.67 and 1.76 eV yields a pattern corresponding well to the experimental data (Figure 3a, b). Similar to the case of a single nanorod, higher order modes pile up at the onset energy of the gold d-band absorption at about 2.4 eV. The spectral overlap caused by strong damping prevents the observation of specific mode pattern at this energy in both, the simulated and experimental EEL maps.

2.3. Binding Angle Independence

A similar good agreement between experiment and simulation as above is found for the EEL spectra and maps for all other investigated nanorod pairs at various binding angles γ, as summarized in Figures S3 (spectra), S9, and S10 (EEL maps) (Supporting Information). **Figure 4** depicts their STEM images and the experimentally measured (dots) and simulated (circles) resonance positions. Despite some scattering, likely due to dimensional variations among the nanorods, the robustness of the resonances against changes in the binding angle is evident. Thus far, our findings confirm that despite some statistical variations in geometry, the plasmonic resonances of nanorod dimers exhibit remarkable invariance with respect to the binding angle, and comparison to simulations suggest that the nanorods within the dimers could be conductively connected.

Nevertheless, since a convincingly good accordance between our experiments and simulations is found, we further investigate the binding angle dependence of resonance positions by simulations. This enables insights that are challenging, if not impossible, to retrieve from experiments alone. On one hand, size variations of nanorods, although small, still lead to some data scattering, which might cover minute changes in the spectral positions. On the other hand, variations in the resonance energies in experimental data caused by the inaccessible details of the gap geometry can be excluded in the simulations. Finally, more geometries can be explored.

We first focus on the binding angle dependence of the BDM and ADM resonances of a nanorod dimer with the simplified assumption of a 1 nm gap without flattening of the caps. Up to now, we defined the binding angle γ, but a closer look reveals the utility to split γ into two angles, α and β, that are measured between the long axes of the nanorods and the connecting line between the centers of the neighboring, hemispherical end caps

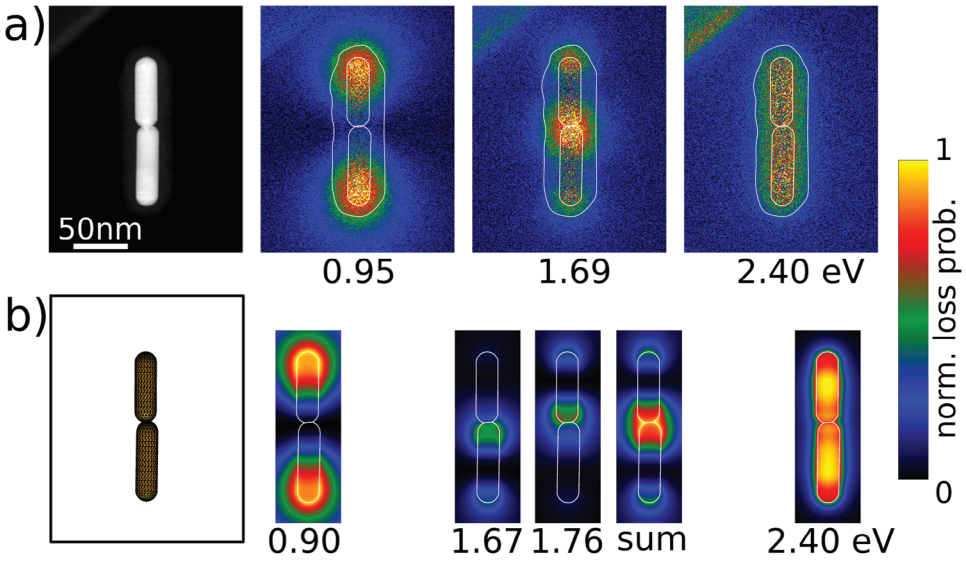

Figure 3. a) Experimentally recorded STEM-ADF image and EEL maps. b) Model and simulated EEL maps for a connected nanorod dimer with the experimental dimensions and −1.5 nm distance in homogeneous environment with n=1.33. Numbers below the images indicate the energy in eV. Where two values are given, the image is the sum of the two corresponding individual images.

(**Figure** 5c). The results of the simulations over the possible angular ranges $0 < \alpha < 90°$ and $-90° < \beta < 90°$ are presented in Figure 5. Indeed, over a large angular range, we find only very weak changes in the resonance energies, with slightly larger deviations for the BDM as compared to the ADM. For the symmetric configuration ($\alpha = \beta = \gamma/2$, dotted lines in Figure 5a,b), the angular dependence is plotted in Figure 5d. Up to $\alpha = \beta = 80°$, the ADM changes less than 1% and the BDM less than 3% with respect to the value at $\alpha = \beta = 0°$. In Figure 5e,f, we plot the charge distributions calculated for the ADM and BDM quasi-static eigen-modes. The charge patterns on the nanorods basically resemble those of the individual nanorods dipolar modes, albeit coupled symmetrically (BDM) or anti-symmetrically (ADM). Upon closer examination, there are of course deviations in the gap region, with the charges being repelled outwards (ADM) or attracted inwards the gap (BDM). More pronounced deviations from the charge distribution of individual rods are observed for angles of 80° and above. At $\alpha = \beta = 90°$, the BMD charge distribution resembles more that of a gap mode between two parallel rods and the similarity to the individual rods dipolar modes has disappeared.

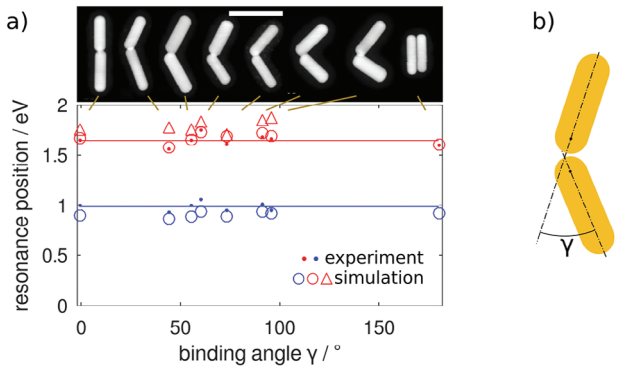

Figure 4. STEM-ADF images and spectral position of the observed resonances of nanrod dimers as a function of the binding angle γ from experiment (dots) and simulations (blue circles, red circles and red triangles for the main three resonances observed in the spectral range between 0.8 and 2.5 eV). The resonances energies are independent of the binding angle. The horizontal red and blue lines are guides to the eye.

Qualitatively, this behavior can be understood by considering the specific mode- and coupling situation of nanorod dimers. The longitudinal dipolar modes (LDM) for the elongated nanorod shapes as considered here are at relatively low energies and spectrally far from all other plasmonic modes. Consequently, when bringing two nanorods together, they predominantly interact (hybridize) with each other, whereas other modes have little influence because they simply are energetically too far to be coupled at a reasonable strength. Furthermore, the LDM exhibit surface charge distributions that are concentrated to the end-caps of the nanorods, accompanied by electric fields that decline rapidly with distance from the end faces. In the stretched end-to-end configuration the interaction between the LDMs of both nanorods is thus governed by the charges at the neighboring gap-side ends, and the influence of the far ends is weak. This reasoning also applies to other binding angles. Assuming a $1/d_c$ interaction potential (with d_c being the distance between the center of mass of the opposite charges) and a distance between the far ends of about ten times larger than between the close ends, it can be expected that additional interaction energies and resonance shifts to be limited to below 10% of the resonance shift at the stretched configuration. This is indeed fulfilled over a wide angular range: Starting from $\alpha = \beta = 0°$, the overlap of the LDM mode electric fields decreases with increasing α and β, which explains the reduced splitting with increasing angles up to about 60° (Figure 5d). Beyond this point, the trend reverses. The interaction between the now approaching far ends and the obvious changes in the mode's charge distribution (Figure 5e,f) become the dominant factors influencing the angle-dependent LDM-splitting in this range.

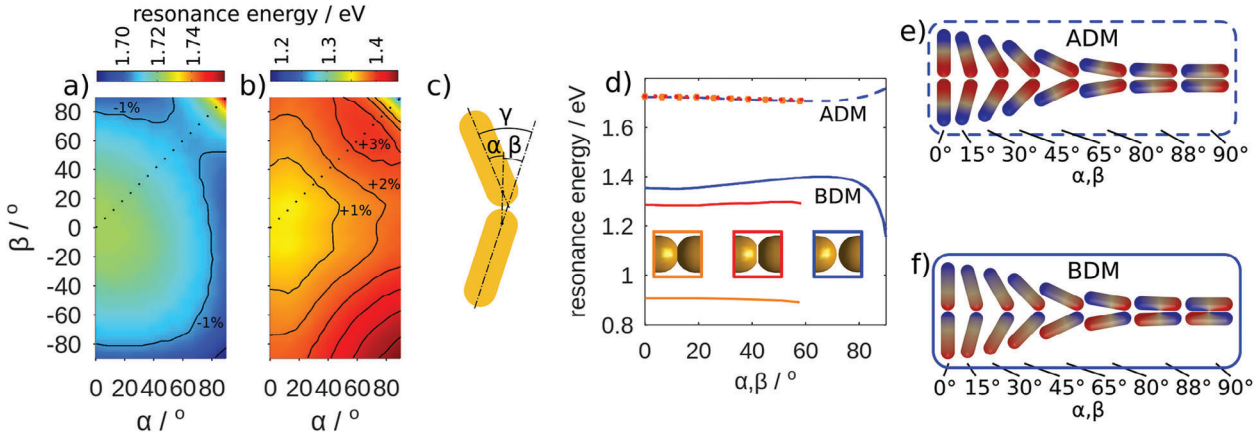

Figure 5. Resonance position of a) the BDM and b) the ADM of a nanorod dimer with 1 nm gap as sketched in c). d) Resonance energies of the BDM and ADM for symmetric configurations $\alpha = \beta$. Blue lines: 1 nm gap, no flattening; red lines: 1 nm gap, flattened rod ends, nominal distance −1.5 nm; orange lines: conductive contacting rods, nominal distance −1.5 nm. e,f) depict the simulated charge distributions for the BDM and ADM of a nanorod pair with 1 nm gap (no flattening). Up to about 80°, the charge distributions on the individual rods resemble that of dipolar excitations, except for a very small area in the gap.

When the rods are finally in the side-by-side configuration, the interaction energy and mode splitting are expected to be roughly double of that of the stretched end-to-end configuration, as now both ends interact with identical strength. To illustrate this point, we vary the binding distance at the end-to-end and the side-by-side configuration for fixed binding angles of $\alpha = \beta = 0°$ and $\alpha = \beta = 90°$ and calculate the ADM and BDM energies. **Figure 6** compares the results of both mode-dispersions. The blue and red dots in Figure 6e indicate the resonance energy shifts of the end-to-end configuration multiplied by two, which we find to be in excellent agreement with the resonance energies of the side-by-side configuration (dashed lines). Despite its simplicity, this approach provides a reasonably good explanation for the observed angle-dependent resonance shifts or -invariances. Nevertheless, at distances below ≈ 10 nm, the simulated charge distributions deviate strongly from those of the individual nanorods in the side-by-side configuration. The interaction over the entire gap along the nanorod sides leads to the formation of gap modes that cannot be considered as a weak perturbation of the modes on individual particles. In a simplified dipole model, where the energy shifts are proportional to the interaction energy of the charges, a $1/d_c$ dependence of the energy shifts is expected, with d_c being the distance between the center of mass of the opposite charges. Assuming that the center of mass of the charges is located between the rod end and the center of the hemispherical caps (here, 2 nm from the ends for the BDM and 7 nm from the ends for the ADM), we find a very good agreement between this model and the simulation results (red and blue + symbols in Figure 6e).

The question arises, to what extent the observed independence of LSPR energy on binding angle also holds for configurations with flattened or conductively connected ends. Simulations show that the robustness of the resonance energies against angle variations is maintained in these cases as well. This is illustrated in Figure 5d for nanorod dimers in symmetric configurations (α=β) with flattened and conductively connected ends (the resonance positions over the full angular range are found in Figure S11, Supporting Information). The binding angle robustness of nanorod dimer resonances is a general phenomenon

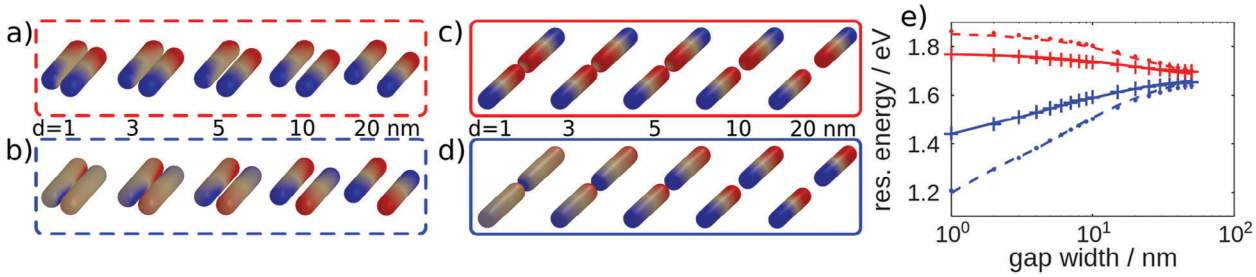

Figure 6. a–d) Charge distributions of ADM and BDM quasi-static eigen-modes at the particles surfaces for varying distances. The rod diameter was set to 20 nm and their length to 70 nm. e) Resonance energies as a function of rod distance of BDM (blue) and ADM (red) for the end-to-end configurations (solid lines) and the side by side configurations (dashed lines). The dots show the values calculated by doubling the resonance shifts of the end-to-end configurations with respect to a reference energy of 1.67 eV. The +-symbols show the resonance shifts as calculated from a simple model presuming an $1/d$ potential, $E_{res}(d) = E_{res,0} d_0/d_c$ with $E_{res,0}$ being set to the simulated resonance shift at $d_0 = 1$ nm gap width, d_c is the distance between the center of mass of the charges on the opposite sides of the gap. d_c was chosen to fit the simulated curves with $d_c = d_{gap} + 4$ nm for the BDM (charges at opposite sides of the gap have opposite sign and attract each other) and $d_c = d_{gap} + 14$ nm for the ADM (charges at opposite sides of the gap have the same sign and repel each other, thus they are slightly pushed apart).

that does not depend on the exact gap- or contact geometries and might prove useful for the understanding of larger assemblies as, e.g., nanorod chains. End-to-end dimerized nanorods excel in this regard against other mutual orientations[19] or bent nano-wires[20], which do show significant angle dependence of the LSPR. The reason for this difference lies in the dominant coupling via the narrow gap or the significant constriction at the binding rod ends. The latter forces a charge-node of the LSPR modes, a condition not present in bent nano-wires.

3. Conclusion

In conclusion, by combining experiments and numerical simulations, we confirm the invariance of nanorod dimer resonances over a large range of binding angles. We explain this behavior by two main features of nanorod dimers: a) Over a large range of binding angles, the neighboring ends are much closer to each other than to the far ends and thus interaction is mostly mediated by the neighboring ends only. This is clearly illustrated by an analytical charge coupling model. b) Plasmonic multi-polar and transversal dipole modes are energetically well separated from the longitudinal dipole modes, which thus couple dominantly with each other, again practically independent of the binding angle. However, approaching the side-by-side configuration, the coupling strength increases significantly. Here, the interaction between the far ends becomes equivalent in strength to that of the nearby ends, thus roughly doubling the mode splitting as compared to the end-to-end configuration. Additionally, strong multi-polar mode hybridization and gap mode formation are not negligible. The weak angle dependence of the resonance and the high stability of silica-coated dimers, together with the large surface enhancements in designable, rod-length dependent spectral ranges renders nanorod dimers a potentially important structure for surface-enhanced spectroscopies, provided that geometry and distance control can be further improved and the gap made accessible to the analyte of interest.

4. Experimental Section

Nanorod Synthesis and Assembly: Gold nanorods and nanorod dimers were synthesized according to the scheme published in ref. [6]. Single crystalline nanorods with hemispherical caps were synthesized following a standard protocol, resulting in a quite narrow distribution in nanorod length and diameter of 69 ± 10 nm and 21 ± 4 nm, respectively. The longitudinal plasmon resonance was at a resonance energy of around 1.58 eV (785 nm). Trans-1,2-bis(4-pyridyl)ethylene (BPE) was employed as a bifunctional coupling agent to connect two nanorods.[21] The assembly process of the nanorods began by introducing BPE into the colloidal nanorod solution. Then, the assembly in solution was halted by introducing silver nitrate. STEM images evidence the dimerization of the nanorods at their tips.[21] Subsequently, the resulting dimers were encapsulated with a mesoporous silica layer (average thickness over all investigated particles: 12.5 ± 1.7 nm) to enhance their stability over time. Electron microscopy analysis confirmed that, after encapsulation in the silica shell, the variable angles between end-to-end dimers were preserved in different relative orientations.[6] Notably, the predetermined angle between two rods was established during the solution phase and was not a result of the drying process on the imaging substrate. It was worth mentioning that without the addition of silver nitrate, the encapsulation in the silica shell led to a substantial proportion of nanorod chains consisting of more than five nanorods. Conversely, employing silver nitrate before the growth of the silica layer proved to be the most effective strategy for obtaining well-defined and long-term stable silica-encapsulated nanorod dimers.The BPE-mediated binding and the silica shell were expected to ensure a constant gap size of 1 nm in all cases.

STEM-EELS: The gold nanorod dimers were deposited randomly by capillary action from a drop of the solution, on the ultra-thin carbon membrane of a TEM Cu grid, which was subsequently degassed at 100°C for 2 h prior to insertion in the TEM column. EELS experiments had been carried out in STEM mode in a double-corrected FEI Titan Cubed 80-300 (S)TEM operated at 80 kV, equipped with a monochromator and a GIF Quantum ERS imaging filter. The monochromator was adjusted to reach an energy resolution of 90 meV. The spectra were acquired with a dispersion of 0.01 eV per channel. In STEM-EELS, the electron beam was raster scanned across the sample and EEL spectra were recorded for each beam position. 3D data cubes were acquired using the Spectrum Imaging acquisition routine implemented in Gatan microscopy suite 2. Data set sizes were 200×248 pixels^2 for the single nanorod, and 260×330 pixels^2 for two nanorods. The spectra were realigned in energy, and the intensity was normalized to the zero-loss peak. Subsequently, 2D maps for specific loss energies were sliced from the data cube. Slices of 20 meV range were centered on specific LSPR energies. The energy and contrast ranges were user-defined within Gatan microscopy suite three to optimally isolate specific LSPR modes in the EELS maps.

Simulations: Simulations were performed by the freely available MNPBEM17 Matlab toolbox.[22,23] Literature values for the dielectric functions of gold,[24] SiO_2[15] and carbon[25] were used. For the simulations the nanorods were modeled according to the actual dimensions as measured from the STEM images, however presuming a rotational symmetric shape along the nanorod axis as well as a hemispherical end cap geometry, which both were just approximations to the nanoscopic shape.[16,26] If not noted differently, EEL spectra were calculated in the case of monomers for a beam position 5 nm from the end of the nanorod or, in the case of the dimers, 5 nm from the end of the shorter nanorod on the nanorod axis.

Supporting Information

Supporting Information is available from the Wiley Online Library or from the author.

Conflict of Interest

The authors declare no conflict of interest.

Data Availability Statement

The data that support the findings of this study are available from the corresponding author upon reasonable request.

Keywords

EELS, gold nanorod dimers, plasmonics

Received: April 4, 2024
Revised: May 29, 2024
Published online:

[1] N. Zohar, L. Chuntonov, G. Haran, *J. Photoch. Photobio. C* **2014**, *21*, 26.
[2] X. Lu, D. Punj, M. Orrit, *Nano Lett.* **2022**, *22*, 4215.
[3] R. Esteban, G. Aguirregabiria, A. G. Borisov, Y. M. Wang, P. Nordlander, G. W. Bryant, J. Aizpurua, *ACS Photonics* **2015**, *2*, 295.

[4] H. Chen, L. Shao, Q. Li, J. Wang, *Chem. Soc. Rev.* **2013**, *42*, 2679.
[5] A. Kar, V. Thambi, D. Paital, G. Joshi, S. Khatua, *Langmuir* **2020**, *26*, 9894.
[6] I. Haidar, G. Lévi, L. Mouton, J. Aubard, J. Grand, S. Lau-Tourong, D. R. Nueville, N. Félidj, L. Boubekeur-Lesaque, *Phys. Chem. Chem. Phys.* **2016**, *18*, 32272.
[7] M. Kim, H. Kwon, S. Lee, S. Yoon, *ACS Nano* **2019**, *13*, 12100.
[8] A. K. Sahu, S. Raj, *Gold Bull.* **2022**, *55*, 19.
[9] L. Shao, K. C. Woo, H. Chen, Z. Jin, J. Wang, H.-Q. Lin, *ACS Nano* **2010**, *4*, 3053.
[10] M. R. Shcherbakov, A. T. Le, N. Dubrovina, A. Lupu, A. Fedyanin, *Opt. Lett.* **2015**, *40*, 1571.
[11] M.-W. Chu, V. Myroshnychenko, C. H. Chen, J.-P. Deng, C.-Y. Mou, F. Javier Garcia de Abajo, *Nano Lett.* **2009**, *9*, 399.
[12] J. Nelayah, M. Kociak, O. Stephan, F. J. Garcia de Abajo, M. Tence, L. Henrard, D. Taverna, I. Pastoriza-Santos, L. M. Liz-Marzan, C. Colliex, *Nat. Phys.* **2007**, *3*, 348.
[13] M. Bosman, V. J. Keast, M. Watanabe, A. I. Maaroof, M. B. Cortie, *Nanotechnology* **2007**, *18*, 16.
[14] D. Rossouw, M. Couillard, J. Vickery, E. Kumacheva, G. A. Botton, *Nano Lett.* **2011**, *11*, 1499.
[15] I. H. Malitson, *J. Opt. Soc. Am.* **1965**, *55*, 1205.
[16] H. Katz-Boon, C. J. Rossouw, M. Weyland, A. M. Funston, P. Mulvaney, J. Etheridge, *Nano Lett.* **2011**, *11*, 273.
[17] L. A. Jakob, W. M. Deacon, Y. Zhang, B. de Nijs, E. Pavlenko, S. Hu, C. Carnegie, T. Neuman, R. Esteban, J. Aizpurua, J. J. Baumberg, *Nat. Commun.* **2023**, *14*, 3291.
[18] A. Campos, N. Troc, E. Cottancin, M. Pellarin, H.-C. Weissker, J. Lerme, M. Kociak, M. Hillenkamp, *Nat. Phys.* **2019**, *15*, 275.
[19] C. Tabor, D. Van Haute, M. A. El-Sayed, *ACS Nano* **2009**, *3*, 3670.
[20] E. P. Bellido, I. C. Bicket, G. A. Botton, *Nanophotonics* **2022**, *11*, 305.
[21] I. Haidar, J. Aubard, G. Lévi, S. Lau-Truong, L. Mouton, D. R. Neuville, N. Félidj, L. Boubekeur-Lecaque, *J. Phys. Chem. C* **2015**, *119*, 23149.
[22] U. Hohenester, A. Truegler, *Comput. Phys. Commun.* **2012**, *183*, 370.
[23] U. Hohenester, *Comput. Phys. Commun.* **2014**, *185*, 1177.
[24] P. Johnson, R. Christy, *Phys. Rev. B* **1972**, *6*, 4370.
[25] E. T. Arakawa, M. W. Williams, T. Inagaki, *J. Appl. Phys.* **1977**, *48*, 3176.
[26] B. Goris, S. Bals, W. Van den Broek, E. Carbo-Argibay, S. Gomez-Grana, L. M. Liz-Marzan, G. Van Tendeloo, *Nat. Mater.* **2012**, *11*, 930.